RSC Advances

ROYAL SOCIETY OF CHEMISTRY

www.rsc.org/advances

Journal Name

COMMUNICATION

C/Si/core-shell structured TiO_2@TiO_{2-x} nanocomposites with excellent visible-light photocatalytic performance

Received 00th January 20xx,
Accepted 00th January 20xx

DOI: 10.1039/x0xx00000x

www.rsc.org/

Shunhang Wei [a], Rong Wu [a,*], Jikang Jian [b], Yanfei Sun[a]

C/Si/core-shell structured TiO_2@TiO_{2-x} nanocomposites were obtained by combining C, Si and black TiO_2. Amounts of Ti^{3+} and oxygen vacancies in TiO_2@TiO_{2-x} and electron transfer among C, Si and TiO_2@TiO_{2-x} inhibited electron/hole recombination, which resulted in excellent photocatalytic performance.

The growing concern around water pollution has put greater stress on the need to develop ways of removing hazardous chemical compounds from water. TiO_2 is the most widely used photocatalyst for environmental purification because of its favorable properties such as cost-effectiveness, and long-term stability against photocorrosion and chemical corrosion.[1,2] However, fast electron–hole recombination and the wide bandgap of conventional white TiO_2 photocatalyst (3.2 eV for anatase) significantly limit its practical application.[3] With this view, modification of TiO_2 has been undertaken by many researchers. The emergence of black TiO_2 has a significance of milestone as the above two drawbacks have been largely solved. Especially, the core-shell structured black titania has better photocatalytic performance.[4] In spite of this, the photodegradation efficiency of sole TiO_2 is still not very good since it needs around 180 minutes to degrade around 40% of the concentration of pollutant after adsorption/desorption equilibrium under visible-light irradiation.[4,5] In recent research, heterogeneous photocatalyst is an effective method for developing photocatalysis to deal with environmental pollution problems.[6,7] Hence, we attempt to obtain a new black titania-based nanocomposite with better visible-light degradation performance through faster electron transportation.

Recently, functional carbonaceous materials serving as an intercomponent deposited onto the surface of oxides have attracted much attention, because they can modify the corrosion resistance, thermal stability, adsorbability, or electronic properties of these materials. Among them, carbon can act as a sensitizer through generating and transferring electrons under visible light irradiation. Several TiO_2 systems modified with carbon have been reported recently and exhibit significantly enhanced photocatalytic performance.[8-10] Therefore, carbon is able to become an excellent selected material for composite.

On the other hand, silicon, an abundant material on Earth, has a narrow band gap for the broad absorption of sunlight. The conductive band of Si is more negative than TiO_2, which benefit to electron transportation. Embedding Si into TiO_2 is found to form new physicochemical properties such as high thermal stability and good surface wettability.[11] Low carrier-recombination centers and narrowing the band gap of TiO_2 via Si 3p states effectively mixed with O 2p states are benefit to develop the photocatalysis of titania based composites.[12,13] Based on recent research, TiO_2 consisting of silicon also shows advantages for water purification.[11,14-16]

In the present study, given the advantages of C and Si to titania, we report a facile method to prepare a C/Si/ core-shell structured TiO_2 compound with excellent visible-light photodegradation efficiency. In this method, the experience obtained through the preparation of black titania is drawn on. The colloid as titania precursor is obtained from the preparation method for black titania, as reported previously.[17] The mixture of the colloid , silicon and sucrose are heated under N_2 or air atmosphere to produce the composite material. The nanocomposite overcomes the drawbacks of sole TiO_2 and integrates the advantages of each respective component, as it exhibits not only high visible-light photodegradation efficiency but also excellent visible-light absorption.

The X-ray diffraction (XRD) patterns of the CST(N_2) and CST(air) samples are presented in Fig. 1a. The diffraction peaks at 25.2°, 37.8°, 54°, 55°, 62.7° and 68.8° are assigned to the (1 0 1), (0 0 4), (1 0 5), (2 1 1), (2 0 4) and (1 1 6) reflections of anatase TiO_2, respectively. The diffraction peaks at 28.4°, 47.3°, 56.1°, 69.1° and 76.3° are assigned to the (1 1 1), (2 2 0), (3 1 1), (4 0 0) and (3 3 1) reflections of Si, respectively. As expected, the XRD patterns of the nanocomposites clearly match with the structures of Si and TiO_2, confirming the presence of Si and TiO_2 in the nanocomposites. As can be seen clearly, some diffraction peaks of TiO_2 are not

[a] Key Laboratory of Solid-state Physics and Devices, School of Physical Science and Technology, Xinjiang University ,Urumqi830046,China. E-mail: wurongxju@sina.com
[b] School of Physics and Optoelectronic Engineering, Guangdong University of Technology, WaiHuan Xi Road, No. 100, Guangzhou 510006, China.
Electronic Supplementary Information (ESI) available: Experimental details, XPS and Physical and Structural Properties of samples

distinguishable in the XRD patterns of CST(N_2) nanocomposite. This can be ascribed to the much lower crystalline extent of TiO_2 than that of Si, which results in the shielding of some peaks of TiO_2 by those of Si.

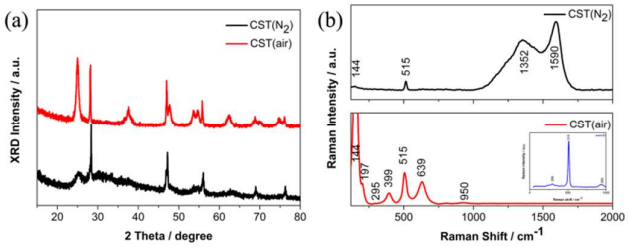

Fig. 1 XRD patterns (a) and Raman spectra (b) of CST(N_2) and CST(air)

Raman spectroscopy is employed to ensure the presence of carbon material. Fig. 1b exhibits the Raman spectra of CST(N_2) and CST(air). For the CST(N_2)sample, the G band (1590 cm^{-1}) corresponding to sp^2 hybridized carbon and the D band (1352 cm^{-1}) originating from disordered carbon can be observed.[18] In addition, the strongest peak of anatase titania should be located at ~144cm^{-1}, but the peak at 515cm^{-1} shown in Figure 1b is stronger. Therefore, the peak should be assigned to the 515 cm^{-1} band of elemental silicon superimposed with the 515 cm^{-1} band of anatase titania.[19] In contrast, CST(air) exhibits six Ramanactive modes of anatase titania with frequencies at 144, 197, 399, 515, 519 (superimposed with the 515 cm^{-1} band), and 639 cm^{-1}, and three modes of silicon with frequencies at 295, 515 and 950cm^{-1}.[3,19] However, the D band and G band do not occur in this spectrum, which indicates a failure of incorporating C into Si/TiO_2. This may be attributed to intense disruption of C in CST(air), which leads to C doping into TiO_2 rather than formation of a C/Si/TiO_2 compound.

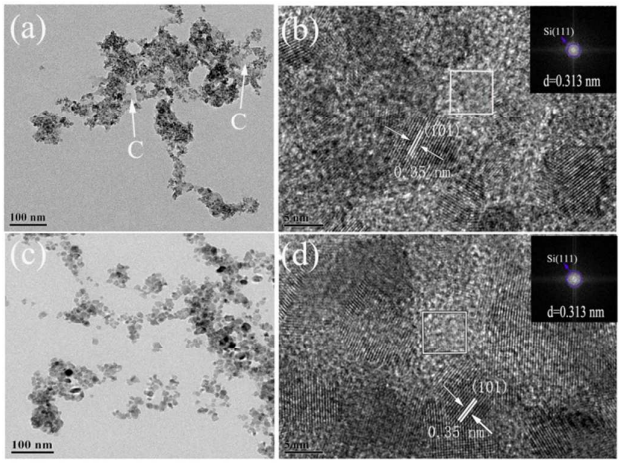

Fig. 2 (a) TEM image of CST(N_2), (b) HRTEM micrographs of CST(N_2), (c) TEM image of CST(air), (d) HRTEM micrographs of CST(air)

The morphology and crystalline microstructure of CST(N_2) and CST(air) are confirmed by TEM (Fig. 2a and c). Fig. 2a shows that a lot of darker nanoparticles are deposited onto the carbon layer. However, the carbon layer does not appear in Fig. 2c. From the results of the high resolution transmission electron microscopy (HRTEM) (Fig. 2b and d), these darker nanoparticles are demonstrated as the composite of silicon and TiO_2. In the HRTEM image and the corresponding fast Fourier transform (FFT), clear lattice fringes with spacings of 0.35 nm and 0.313 nm are observed, corresponding to the (101) crystallographic plane of TiO_2 and the (111) crystallographic plane of the silicon, respectively. The results also illustrate that carbon fails to combine with Si/TiO_2 in CST(air).

Fig. 3a shows the Fourier transform infrared spectroscopy (FTIR) of CST(N_2) and CST(air). The absorption bands centered at 3388 cm^{-1} and 1616 cm^{-1} can be attributed to stretching and bending vibrations of hydroxyl groups, respectively.[20] For the CST(N_2) sample,
the peaks assigned to the C-O-C vibration and Si-O-Si stretching bond at 1119 and 1250 cm^{-1} can be observed clearly, implying the presence of Si and carbon.[21]

The optical absorption property of CST(N_2) and CST(air) is measured by UV-vis spectroscopy. As shown in Fig. 3b, it is clear that CST(air) can absorb considerable amounts of visible light, as a broad absorption band in the range of 330-800 nm can be observed in the absorption spectra. Notably, after the successful addition of carbon to the Si/TiO_2 compound , CST(N_2) can absorb more visible light than CST(air), as the absorption edges of CST(N_2) are a significantly red shifted to around 756 nm. This may be ascribed to the introduction of carbon modifying the fundamental process of electron-hole pair formation and resulting in an increased electric surface charge of the oxide within the composite.[22] In addition, according to previous research, the enhanced light absorption may be partly ascribed to the introduction of Ti^{3+} and oxygen vacancies.[5,17]

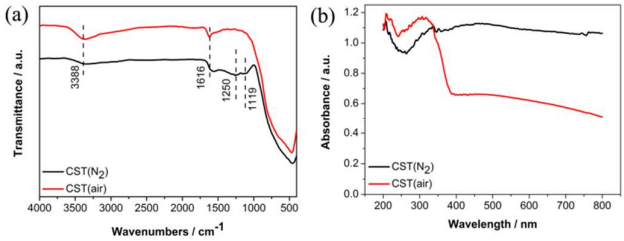

Fig. 3 FTIR spectra (a), Spectral absorbance (b) of CST(N_2) and CST(air)

The presence of Ti^{3+} in our samples is supported by electron paramagnetic resonance (EPR) spectroscopy, shown in Fig. S1 (ESI). Obviously, CST(N_2) samples exhibit strong EPR signal with a g-value of ~2.002, which assigned to Ti^{3+}.[4,5,17,23] Hence, the results verify that Ti^{3+} and oxygen vacancies are introduced into the CST(N_2) sample. In contrast, the signal is not exhibited in CST(air).

The compositional and structural information of CST(N_2) and CST(air) are characterized using X-ray photoelectron spectroscopy (XPS), as shown in Fig. 4. The C 1s peak of CST(N_2) can be deconvoluted into three peaks. The peak of 284.7 eV corresponds to sp^2 carbon. The additional peaks observed for the sample at 285.5 and 287.9 eV correspond to the carbon attached to oxygen atoms and reflect the formation of defects in the CST(N_2). These defects are attributed to C-O and C=O, respectively, and can easily bind to the surface hydroxyl groups of titania to form Ti–O–C bonds,

which impart visible light activity to the titania.[24-26] In contrast, the three different peaks of CST(air) located at 284.8, 286.2 and 288.8 eV are attributed to C-C (sp^2 carbon), C-O, and O=C-OH, respectively.[27] The results confirm our assumption that C doping into TiO_2 through intense disruption of carbon annealed in air. Fig. S2a and b (ESI) show XPS spectra for the Ti 2p binding energy region. The bands located at binding energies of 458.6 eV and 464.3 eV for CST(air) are ascribed to the Ti^{4+} chemical state. Obviously, the binding energy of Ti 2p of CST(N_2) has shifted from 458.6 to 459 eV, and from 464.3 to 464.7 eV. Simultaneously, the O 1s and Si 2p binding energies of CST(N_2) are not only higher than that in CST(air) but also accompanied by the formation of further peaks centered at 533.1 eV and 100.2 eV. These are evidence for the formation of Si-O-Ti and Si-O-Si. Given that the electronegativity of Si is greater than that of Ti, electron density around Ti atom decreases and results in an increase in the binding energy of Ti.[28] Meanwhile, the shortening of the Ti–O bond leads to an increase in the binding energy of O atoms.[29] These results indicate that Ti^{4+} cations insert into the silicon network to form Ti–O–Si linkages.[29] In addition, the electronegativity of O is greater than that of Si, which leads to increases in the binding energy of Si. The formation of Si-O-Si is supported by the binding energy of oxygen at 533.1 eV and consistent with FTIR results.[30] Interestingly, no peaks of Ti^{3+} are found in the XPS of the CST(N_2) samples, which may be assigned to the detection distance (ten atomic layers) for XPS.[4] In other words, a core – shell structure signed as TiO_2 @ TiO_{2-x} is formed. The shell structure is hardly recognizable in the HRTEM image, which may be ascribed to the overlap between Si and TiO_2.

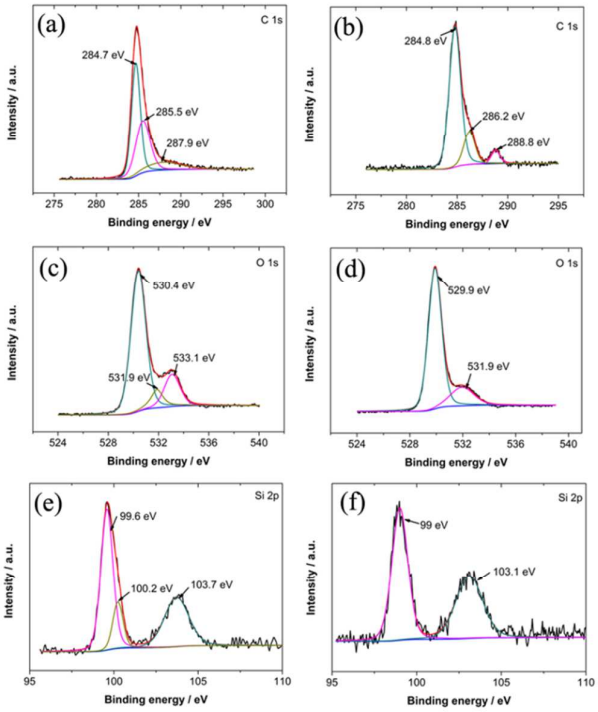

Fig. 4 XPS spectra for (a) C 1s of CST(N_2), (b) C 1s of CST(air), (c) O 1s of CST(N_2), (d) O 1s of CST(air), (e) Si 2p of CST(N_2) and (f) Si 2p of CST(air).

Photoluminescence (PL) emission spectra are used to understand the charge separation and recombination behavior, and migration efficiency of the two samples. Fig. 5a exhibits the PL spectra of CST(N_2) and CST(air) under 240 nm light excitation at room temperature. Clearly, the PL intensity of CST(air) is much higher compared with that of CST(N_2). This indicates that CST(N_2) has a relatively low recombination rate of electrons and holes, which benefit to improve photocatalytic activity.[5]

Methylene blue (MB) was selected as model pollutant to evaluate the photocatalytic activity of the CST(N_2) and CST(air) samples under visible light irradiation. Before turning on the visible light, the mixed suspension of MB and catalyst is magnetically stirred for 180 min to achieve the equilibration of absorption and desorption. Fig. 5b shows that CST(N_2) sample is markedly higher for the MB adsorption amount, as most dye molecules(*ca.*93.73%) remain in the solution with CST(air) as the catalyst (see Table 1 in ESI). As shown in Fig.5c, the MB degradation/removal with the CST(N_2) sample exhibits better photocatalytic activity than the CST(air) sample under visible-light irradiation. For CST(N_2), the degradation of MB reaches 79.62% after 120 minutes of visible light irradiation, whereas CST(air) only decomposes by approximately

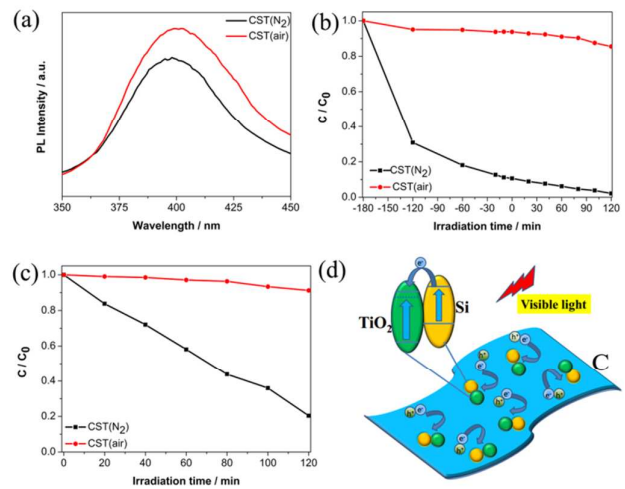

8.79%. Therefore, the degradation rate of the composite has greatly improved compared with sole black titania.

Fig. 5 (a) PL emission spectra of samples (b) Photodegradation of MB in 120 min over CST(N_2) and CST(air), (c) Comparison of MB degradation over different samples under visible light (absorbance at a particular time and that at initial concentration of MB after adsorption equilibrium are denoted as C and C_0, respectively.), and (d) Schematic diagrams of the photoinduced charge separation and migration processes.

The high absorption of visible-light and contaminant, and lower electron/hole recombination rate result in remarkable enhancement of the photocatalysis. A schematic illustration of the mechanism of enhanced photocatalytic performance of CST(N_2) is shown in Fig. 5d. The conduction band (CB) of anatase TiO_2 is −0.24 V (vs. SHE), while the potential of Si is around −0.46 V (vs. SHE).[31,32] In addition, large numbers of Ti^{3+} and oxygen vacancies result in localized oxygen vacancy states just below the conduction band of

TiO_2, which lowers the position of the CB.[17,33] Hence, the photoinduced electrons on the CB of Si can be more smoothly transferred to TiO_2 under visible-light irradiation. On the other hand, the surface carbon can act as a sensitizer, which generates electrons under visible light irradiation and then transfers these electrons to the conduction band of TiO_2 through Ti–O–C bonds.[25,34] This process can greatly enhance the transfer efficiency of photo-generated carriers. At the same time, amounts of oxygen vacancies located at TiO_2 effectively inhibits the recombination of photoinduced e^- and h^+. Thus, a larger number of electrons on the TiO_2 surface and holes on the Si and C surface can participate in photocatalytic reactions to decompose MB, which results in enhanced photocatalytic activity.

Conclusions

In summary, a C/Si/core-shell structured TiO_2@TiO_{2-x} nanocomposite was successfully synthesized via a new chemical approach. Due to the overlap between Si and TiO_2, the core-shell structured titania can not be identified by HRTEM, whereas the results of EPR and XPS do indicate its formation. The presence of C and Si promote the transference of electrons and separation of e^-/h^+ . The large number of oxygen vacancies in TiO_2 play a vital role in suppressing recombination of electrons derived from self excitation and transference. The synergistic effect of the Ti^{3+} and carbon and silicon is responsible for the excellent visible light photocatalytic activity of CST(N_2) catalyst. It is expected that the new method may provide a novel pathway to wastewater treatment.

Acknowledgment

This work was supported by the Natural Science Foundation for Distinguished Young Scholars of Xinjiang (Grant No. 2013711007) and National Natural Science Foundation of China (Grant Nos. 10864004, 11164026, 51172193).

Notes and references

1 A. Kudo and Y. Miseki, *Chem. Soc. Rev.*, 2009, 38, 253.
2 S.Q. Peng, Y.H. Huang and Y.X. Li, *Mater. Sci. Semicond. Process.*, 2013, 16, 62.
3 X. Chen and S.S. Mao, *Chem. Rev.*, 2007, 107, 2891.
4 Z. Wang, C.Y. Yang, T.Q. Lin, H. Yin, P. Chen, D.Y. Wan, F.F. Xu, F.Q. Huang, J.H. Lin, X.M. Xie and M.H. Jiang, *Energy Environ. Sci.*, 2013, 6, 3007.
5 G.L. Zhu, T.Q. Lin, X.J. Lu, W. Zhao, C.Y. Yang, Z. Wang, H. Yin, Z.Q. Liu, F.Q. Huang and J.H. Lin, *J. Mater. Chem. A*, 2013, 1, 9650.
6 M. Alzamani, A. Shokuhfar, E. Eghdam and S. Mastali, *Mater. Sci. Semicond. Process.*, 2013, 16, 1063.
7 M. R. Hoffmann，S. T. Martin, W. Y. Choi and D. W. Bahnemann, *Chem. Rev.*, 1995, 95, 69.
8 P. Zhang, C.L. Shao, Z.Y. Zhang, M.Y. Zhang, J.B. Mu, Z.C. Guo and Y.C. Liu, *Nanoscale*, 2011, 3, 2943.
9 J.G. Hou, S.Q. Jiao, H.M. Zhu and R.V. Kumar, *Crystengcomm*, 2011, 13, 4735.
10 R. Leary and A. Westwood, *Carbon*, 2011, 49, 741.
11 Y. Su, S.O. Chen, X. Quan, H.M. Zhao and Y.B. Zhang, *Appl. Surf. Sci.*, 2008, 255, 2167.
12 K. Yang, Y. Dai and B. Huang, *Chem. Phys. Lett.*, 2008, 456, 71.
13 X.L. Yan, J. He, D.G. Evans, X. Duan and Y.X. Zhu, *Appl. Catal. B Environ.*, 2005, 55, 243.
14 Y.S. Sakhare, S.V. Bhoraskar, V.L. Mathe and A.U. Ubale, *Mater. Res. Bull.*, 2014, 59, 205.
15 A. Hajjaji, K. Trabelsi, A. Atyaoui, M. Gaidi, L. Bousselmi, B. Bessais and M.A. El Khakani, *Nanoscale Res. Lett.*, 2014, 9, 543.
16 C.Y. Duan, H. Wang, X.M. Ou, F. Li and X.H. Zhang, *ACS Appl. Mater. Inter.*, 2014, 6, 9742.
17 S.H. Wei, R. Wu, J.K. Jian, F.J. Chen and Y.F. Sun, *Dalton Trans.*, 2015, 44, 1534.
18 L.Z. Bai, D.L. Zhao, Y. Xu, J.M. Zhang, Y.L. Gao, L.Y. Zhao and J.T. Tang, *Mater. Lett.*, 2012, 68, 399.
19 M. Li, X.H. Hou, Y.J. Sha, J. Wang, S.J. Hu, X. Liu and Z.P. Shao, *J. Power Sources*, 2014, 248, 721.
20 J. Fang, F.C. Shi, J. Bu, J.J. Ding, S.T. Xu, J. Bao, Y.S. Ma, Z.Q. Jiang, W.P. Zhang, C. Gao and W.X. Huang, *J. Phys. Chem. C*, 2010, 114, 7940.
21 L. Yue, W.H. Zhang, J.F. Yang and L.Z. Zhang, *Electrochim. Acta.*, 2014, 125, 206.
22 Y. Liu, R.Z. Zuo and S.S. Qi, *J. Mol. Catal. A-Chem.*, 2013, 376, 1.
23 J.M. Coronado, A.J. Maira, J.C. Conesa, K.L. Yeung, V. Augugliaro and J. Soria, *Langmuir*, 2001, 17, 5368.
24 H. Ago, T. Kugler, F. Cacialli, W. R. Salaneck, M. S. P. Shaffer, A. H. Windle and R. H. Friend, *J. Phys. Chem. B*, 1999, 103, 8116.
25 B.K. Vijayan, N.M. Dimitrijevic, D. Finkelstein-Shapiro, J.S. Wu, and K.A. Gray, *Acs Catalysis*, 2012, 2, 223.
26 J. Huang, Q. Chang, Y.B. Ding, X.Y. Han and H.Q. Tang, *Chem. Eng. J.*, 2014, 254, 434.
27 J.Y. Jing, Y. Zhang, W.Y. Li and W.W. Yu, *J. Catal.*, 2014, 316, 174.
28 X.L. Yan, J. He, D.G. Evans, X. Duan and Y.X. Zhu, *Appl. Catal. B Environ.*, 2005, 55, 243.
29 Z.J. Li, B. Hou, Y. Xu, D. Wu and Y.H. Sun, *J. Colloid Interface Sci.*, 2005, 288, 149.
30 B.J. Aronson, C.F. Blanford and A. Stein, *Chem. Mater.*, 1997, 9,2842.
31 W. Wang, J. Yu, Q. Xiang and B. Cheng, *Appl. Catal. B Environ.*, 2012, 109, 119.
32 X.Q. Bao and L.F. Liu, *J. Power Sources*, 2014, 268, 677.
33 S.H. Wei, R. Wu, J.K. Jian, J. Hou, F.J. Chen, A. Ablat and Y.F. Sun, *RSC Adv.*, 2015, 5, 40348.
34 Y.C. Liu, M.Y. Xing and J.L. Zhang, *Chin. J. Catal.*, 2014, 35, 1511.

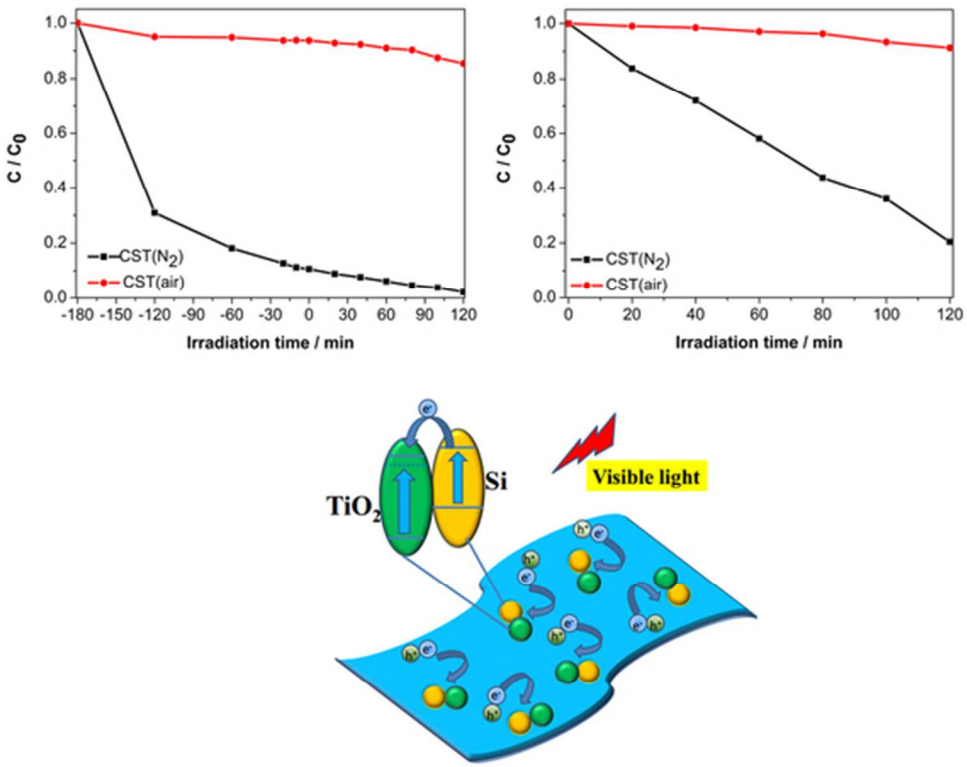

49x39mm (300 x 300 DPI)